Received: 23 January 2021 | Revised: 15 April 2021 | Accepted: 2 June 2021

DOI: 10.1002/suco.202100043

TECHNICAL PAPER

fib CEB-FIP WILEY

Negative bending tests on precast prestressed concrete beams made continuous

Ulla Kytölä | **Olli Asp** | **Anssi Laaksonen**

Unit of Concrete and Bridge Structures, Tampere University, Tampere, Finland

Correspondence
Ulla Kytölä, Unit of Concrete and Bridge Structures, Tampere University, Tampere, Finland.
Email: ulla.kytola@tuni.fi

Funding information
Finnish Concrete Industry

Abstract

The objective of the current study is to investigate and evaluate the flexural behavior of the continuity connection of precast prestressed concrete beams in negative bending when the tendons are located at the compression side. The experimental program included four T-shaped composite cantilever beams which were loaded up to failure. The main variable of the tests was the amount of prestress force of the connected precast beams. The reinforcement ratio of continuity connection was high. The ultimate flexural capacities and moment-curvature relations were calculated theoretically. A comparison was then carried out between both the experimental and theoretical results. These experiments revealed that prestress force did not influence the ultimate hogging moment capacity of the continuity connection, but it had an effect on its soffit's compression cracking and spalling of the concrete cover before failure. This study also indicated that confinement of the concrete had a massive influence on the connection's behavior, and it increased both its negative moment capacity and ductility.

KEYWORDS

Continuity, Prestressed concrete, Precast concrete, Confinement, Moment-curvature

1 | INTRODUCTION

In high-density urban areas, car parks are frequently built beneath the streets, squares and parks. The deck structures of these underground car parks are usually heavily loaded. The loads of the communal deck at ground level consist of many factors, including thick soil layers and traffic loads. Because of this, these deck structures are typically demanding to design and expensive to construct. Precast concrete is a common structural system for normal parking structures. Often single-span, simply supported precast prestressed beams, are however insufficient to carry these heavy deck loads. There is a need to determine ways to improve the application of precast prestressed concrete girders, so that it would be possible to utilize them better in heavy loaded parking deck structures.

In many parts of the world it is typical in bridge construction to increase the capacity of simple span prestressed precast girders by continuity. Simple-span girders are made continuous with a cast-in-place (CIP) deck slabs and connection called diaphragm over the supports. The girders act as simple spans for their own weight load before the connection. After continuity is

Discussion on this paper must be submitted within two months of the print publication. The discussion will then be published in print, along with the authors' closure, if any, approximately nine months after the print publication.

achieved, the composite section of the prestressed beam and CIP deck slab carry the superimposed dead and live loads as a continuous structure. A continuous composite girder offers a great number of advantages over a series of simple spans. In a continuous beam, mid-span bending moments and deflections are reduced. At ULS, over-load will lead to a moment redistribution and failure will occur only when the moment capacity at two or more sections has been exceeded. Consequently, higher robustness can be achieved.[1,2]

A negative moment connection is usually made through a composite CIP reinforced deck. Prestressed beams soffit is conventionally compressed 0.4–0.6 f_c at release. When the effects of the negative bending moment of intermediate supports are added, the bottom flange of multi-span girders is considerably compressed near piers. The situation facilitates high concrete strains in the bottom flange which leads to prestress losses and the fact that prestress force is not fully effective at the girder end. Previous research has established that the compressive stress at the bottom of a simple-span beam made continuous does not come critical if the percentage of decks continuity reinforcement and maximum precompression stress of the girders are low enough. It is commonly suggested that these requirements are met in most composite bridge decks and, as a consequence of that, the prestress force of precast girders may typically be neglected in the negative moment computation of ultimate strength.[1–4] However, less attention has been paid to the behavior of structures (like parking deck structures) which cannot satisfy the conditions described above. How does the high compression in the beams soffit effect the continuity connections negative moment capacity and ductility of the failure?

At Tampere University, a research project founded by the Finnish Concrete Industry studied the potentials of simple-span precast, prestressed concrete girders made continuous in parking deck structures with heavy loads. The majority of the earlier research studies the problem from the standpoint of bridge girders made continuous, where the self-weight of beams is a foremost part of the loads, the negative moment over piers are often lesser and no high permanent soil loads exist. There are only a few studies which introduce experimental results on negative bending tests on precast prestressed beams made continuous. The dimensions, reinforcing and cross-section shapes of these tested specimens have been standard bridge girders that differ from building structures. Recent experimental data about the subject has not been published.[1,2,5]

The objective of this study is to investigate experimentally and analytically the negative moment capacity and ductility of continuity connections of structures, which are applicable to building structures.

2 | TEST PROGRAM

Negative flexural bending tests were conducted up to failure on four T-shaped cantilever girders. The tested girders consisted of two 3 m long rectangular (B × H = 280 × 480 mm^2) precast girders connected by a diaphragm and a deck slab. The degree of prestress of the girders varied and the continuity connections slab parts ratio of reinforcement was chosen to be high. The specimens chosen for this test represent approximately a half scale model of a full scale heavily loaded parking deck structure.

2.1 | Details of precast test beams

Eight precast girders were produced in a prefabrication factory. Two of the test beams were reinforced with ordinary bars and the rest were pretensioned. The prestressed girders contained four (JK4), eight (JK8), or twelve (JK12) bottom strands and all of them had two top strands. The test girders (JK0) were reinforced longitudinally by ordinary bars (2#16), without any prestress force.

The shear reinforcement of each prestressed girder consists of bundled spiral stirrups (H2 #8mm). The spacing of the stirrups was thicker at the beam ends. Non-prestressed beams had closed stirrups and constant spacing. The composite action between precast girders and the cast-in-place deck slab was secured with U-shaped stirrups (H1, #10, c/c = 50 mm) and rough contact surface of the beams was in accordance with EN 1992-1-1 6.2.5. Information concerning the precast beams is given in Table 1 and a detailed reinforcement picture of specimen JK12 is shown in Figure 1. The shear reinforcement of the composite test girders was chosen so that shear failure during testing could be avoided.[6]

2.2 | Details of connected test beams

After manufacturing, the beams were transported to the laboratory of Tampere University to be connected. At precast girder age of 112 days, four girders, each made up of two separate precast girders, were connected by a 650 mm wide diaphragm and a 1500 mm wide and 120 mm thick deck slab. At this stage, the negative flexural strength of the continuity connection was achieved with 36pcs 16 mm and 4pcs 12 mm diameter longitudinal bars. The deck also had a transverse reinforcement (16 mm diameter at 100 mm spacing) to secure the shear strength between the web and flanges of the T-section. The diaphragm and the deck were casted with a concrete mix which was a lower strength class than the one used for the girders. The ends of girders were embedded 200 mm into the diaphragm

TABLE 1 Main characteristics of precast test beams

Girder	Quantity	Identifiers	Prestressed steel in precast girders: Strand quantity per row and row distance from the soffit of the cross section					Precast girders H2 stirrups (#8, 2-bar bundles)
			Row 1: 45 mm	Row 2: 58 mm	Row 3: 106 mm	Row 4: 435 mm	Total	
JK0	2 pcs	JK0-3, JK0-4	0 (2#16)	0	0	0	0	80 pcs c/c = 75 mm
JK4	2 pcs	JK4-5, JK4-11	4	0	0	2	4 + 2	108 pcs c/c = 52 mm, 75 mm
JK8	2 pcs	JK8-9, JK8-15	4	4	0	2	8 + 2	108 pcs c/c = 52 mm, 75 mm
JK12	2 pcs	JK12-12, JK12-14	4	4	4	2	12 + 2	108 pcs c/c = 52 mm, 75 mm

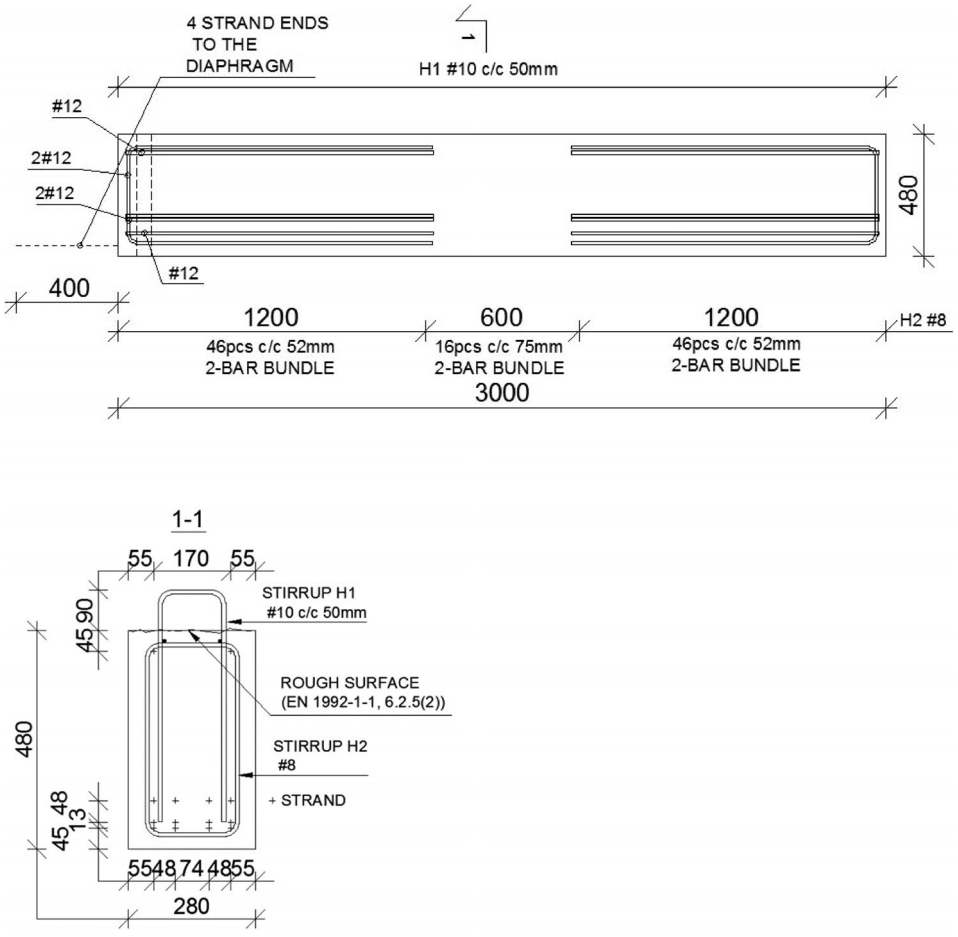

FIGURE 1 Reinforcement drawing of test beam JK12

and four bottom strands were bent into the diaphragm to illustrate a positive moment connection which is commonly used in the continuity connections of precast girders.[7] The diaphragm had a transverse reinforcement according to Figures 2, 3, and 4. A 150 mm high column was added under the diaphragm. Bottom strands were bent into the diaphragm by device which can be seen in the left-hand side of the Figure 4. The dimensions and reinforcement details of test girders are shown in Figure 2, Tables 1 and 2.

2.3 | Material properties

The prestressing steel was seven-wire strand and the effective prestress was 1350 MPa. Wires used in strand were intended. The material properties of the prestressing steel and ordinary reinforcing bars used are presented in Table 3.

The cylinder strength of the concrete used for precast girders was about 70 MPa. The original plan was to use strength class C50/60, but mass prepared in

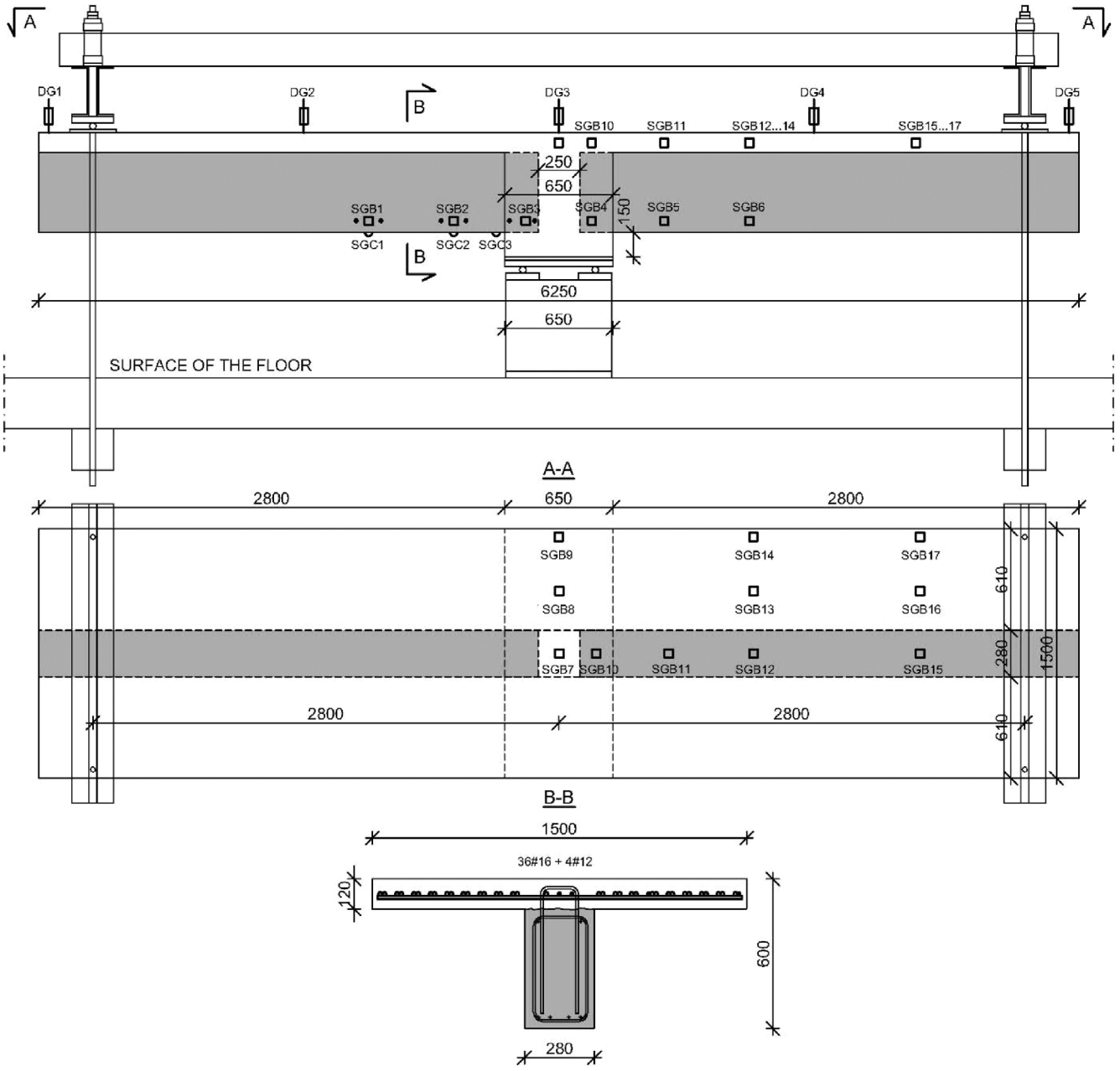

FIGURE 2 Test setup and instrumentation used

the factory increased its strength surprisingly high. Because of that, the deck and diaphragm concrete class was raised from the original plan to cylinder strength 55 MPa. Vibrators were used to densify the concrete. Moist curing under plastic foil took place for the prestressed beams for about 30 h and for the deck and the diaphragm about 7 days. The concrete cylinder strengths are presented in Table 2, based on loading tests of 9–15 pcs field cured cylinders ($d = 150$ mm, $h = 300$ mm) per batch.

2.4 | Instrumentation

Test specimens were measured in two phases, at the precast concrete manufacturing plant at the release of prestress and during a load test at the laboratory. Four different methods of measurement were used.

Concrete and reinforcement strains in the test specimens were measured with electrical and mechanical surface attached strain gauges. The electrical gauges were attached to the reinforcement bars. This measuring

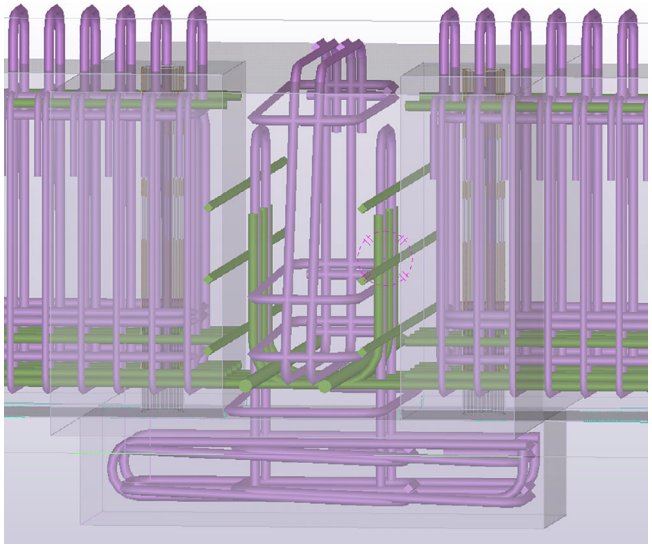

FIGURE 3 3D-model of diaphragm reinforcement[28]

FIGURE 4 Diaphragm during reinforcement work, bent bottom strands and strand bending device

instrument is called a strain gauge bar (SGB) in Figure 2. Uniaxial strain gauges for concrete and mechanical strain gauges (SGC and MSG) were connected on a concrete girder soffit to measure its strains. The strand slip at release of prestress and deformations of the cantilever test beam were measured with displacement gauges. The deformation data of electrical gauges were saved 10 times per second. The locations of such sensors are shown in Figure 2.

2.5 | Test setup

2.5.1 | Tests in precast concrete manufacturing plant

The main purpose of the tests made in the precast manufacturing plant was to determine the transfer length of the specimens, which was supposed to have an influence on the negative bending capacity of the later tested specimens. The data that was to be collected included concrete strains and end slips. Of these measurements, concrete strains turned out to be more accurate. End slip measurements had a large scatter and, because of this, their overall value was limited.

The transfer length on the prestressing strand was measured from five specimens. The results of these tests are presented in Section 3.1. Pre-tension in the beams was released about 30 h after casting, when the cube strength of the concrete was, according to material testing, about 43.6 MPa. Pre-tension force was released gradually and lasted about 15 min.

Two types of strain gauges were used to detect the concrete strains at beam end before and after prestress force transfer. Electrical SGBs used in these measurements contained three measuring points (located at 117, 612, and 1107 mm from beam end) presented in Figure 5. Mechanical strain gauges were also attached on the outside face of the test beam to the same location as the measuring points of the SGBs, to supply additional transfer length data. Mechanical strain gages were read few minutes before prestress force launching and immediately after. At the same time, readings were made once every second with electronical strain gauges. The transfer length could then be estimated by examination of the concrete strain profile.

2.5.2 | Tests in laboratory

During the laboratory's experimental phase, girders were tested in negative bending over a central support. Loading points are presented in Figure 2. The support was directly under the diaphragm, simulating the intermediate support of a continuous girder.

The loads were applied by four displacement controlled 500 kN hydraulic jacks. Two jacks were used at both beam tips, in which case the maximum load was 1000 kN per cantilever. The load was transmitted to the test girder by a separated load shearing beam. Load cells were placed above the load shearing beams to measure the load. The distance between the loads and central support was 2.8 m.

The used loading rate was 50 kN/min and the load steps of 100 kN were used. In every load step visible cracks were highlighted with marker pen. When the load level reached

TABLE 2 Main characteristics of connected girders (tests 5, 6, 7, and 8)

Test no.	Connected precast prestressed girders	Deck slabs ρ_l (%)	Girder age at loading (days)	Slab/diaphragm age at loading (days)	Concrete strength f_{cm} (MPa)	
					Girder	Deck slab
5	JK0-3, JK0-4	5.1	135	23	72.1	54.9
6	JK4-11, JK4-5	5.1	139	27	72.2	55.9
7	JK8-15, JK8-9	5.1	142	30	72.2	56.6
8	JK12-14, JK12-12	5.1	146	34	72.2	57.4

TABLE 3 Reinforcement material properties

Type of reinforcement	Modulus of elasticity Es (GPa)	Yield strength f_y or $f_{p0.1k}$ (MPa)	Area (mm^2)	Tensile strength/ upper yield strength R_m/R_{eH}	Elongation at maximum force A_{gt} (%)
B500B T16	200	547	201	1.167	12.5
Y1860S7–12.5	192	1813	93.2	1.065	6.0

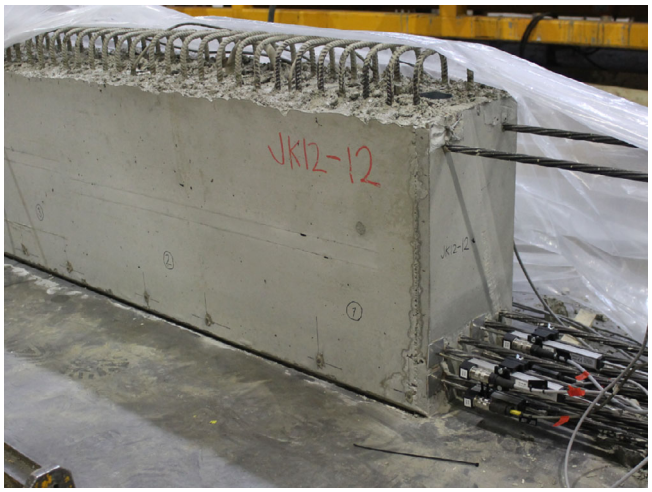

FIGURE 5 Instrumentation of beam JK12 at concrete manufacturing plant

FIGURE 6 Test setup and instrumentation of test 8 at the laboratory

an analytical capacity, researchers only visually observed the test beams from a distance at loading steps and a crack pattern was highlighted after failure. The instrumentation of the load test is presented in Figure 6.

3 | EXPERIMENTAL RESULTS AND DISCUSSION

3.1 | Transmission length

Girder ends strains were measured in the manufacturing plant to gain information on the transmission lengths of test girders. Section 2.5.1 contains the procedures and methods of measuring the strains.

The electrical SGBs and gauge-point measurements yielded congruent results. The measurements were made at three points for every tested beam. According this data, an appropriate estimation of the transmission length of test beams could be made.

The concrete strain profiles obtained are the profiles of the change in concrete strains immediately after the prestress force transfer. Strain profile was drawn through separate measurement locations. All strain profile plots are illustrated in Figure 7. From the plots it can be seen that the strain curve becomes horizontal after the second measurement point (612 mm). Transmission lengths were defined in this study, based on an assumption that the concrete strain grows linearly at transmission length and the transfer of prestress starts immediately from the beam end. Then two lines could be drawn and the point where they intersected was defined as the transmission

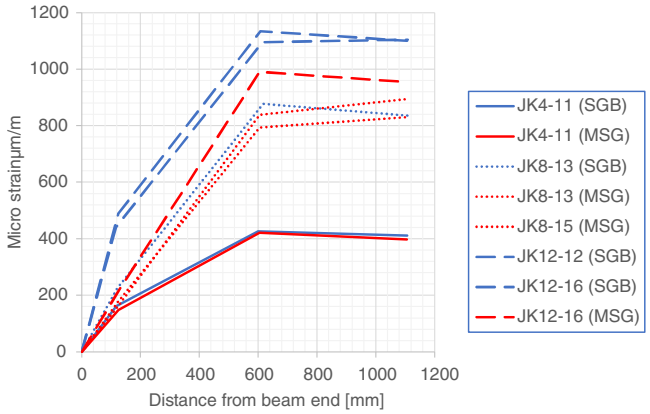

FIGURE 7 Measured prestressing force diagram at test beam end after release

length. The mean transfer length and range were in this study 433 mm and 283–658 mm.

According to EN 1992-1-1, the transmission length of the test beam strands is 751 mm. Experimental test results are in agreement with prior studies, which claim that pretensioned specimens with narrow spaced stirrups, large cross-sections and multiple strands have shorter transfer lengths than minor "transfer length prisms".[8,9]

3.2 | Results of negative moment testing

Before the beginning of the load tests, beams were visually observed. Thin cracks at the slab part of the test specimens, most likely caused by slabs shrinkage/differential shrinkage between the slab and precast beam, were detected already prior to the loading. During loading cross sections, top part flexural cracking increased, and the non-prestressed slab was clearly visually cracked through its whole height already at a load level of 25% of the failure load. According to SGB measurements, deck parts first reinforcement yielded at load level of 66%–69% of the failure load.

At a load level of 67%–89% of the failure load, the first visual cracks were detected at the compressed bottom of test beams about 500 mm away from the centerline of supports. These cracks increased by length strongly, while loading proceeded towards the maximum. Prior to the failure, the concrete cover of cross sections spalled of from the bottom and/or side of each of the test specimens. Although this spalling happened clearly before the ultimate failure in all tests, based on visual observations confined concrete core and reinforcement inside stirrups remained stable up to the reach of structures ultimate capacity. Closely spaced stirrups prevented premature buckling of the compression reinforcement. From the visual observations of the point of fracture a conclusion could be reached that bottom strands and reinforcement had buckled during the failure and stirrups were clearly rounded. Figure 8. shows typical failures experienced by the test beams. The visibly observed point of fracture located in all tests approximately at the same distance from the beam end where the measured transfer zone of the bottom strands, presented in previous section, ended.

It was found in all tests that the diaphragm concrete transferring compression between two precast girders remained undamaged, so that failure always took place outside the diaphragm. In no case did the precast girders pull out of the diaphragm. Horizontal shear strength between the beam and the flanges and at an interface between concrete cast at separate times was also distinguished to be sufficient, as no visible cracking along the contact surface took place between the slab and beam part.

The observed failure mode of the test beams was flexural failure. All girders were clearly controlled by tension, extensive yielding of the slab steel took place before crushing of the concrete, regardless of the prestress effects or the fact that a cross-section was strongly over-reinforced. A cantilever beam developed considerable vertical deflections prior to the failure.

Table 4 shows the following results for the test beams:

1. Visibly observed point of fractures horizontal coordinate (measured from supports centerline) x_{frac1} (mm).
2. Visibly observed point of fractures horizontal coordinate (measured from precast beams end) x_{frac2} (mm).
3. Maximum tested negative moment at the point of fracture M_{test} (kNm).
4. Tested negative moment at onset of visible spalling cracking of beams soffits at the point of fracture $M_{spalling}$ (kNm).
5. Tested negative moment at onset of first yielding of top reinforcement at the point SGB10 M_y (kNm).
6. Vertical deflection at the cantilever tip at failure (mean value of test beams two tips) Δ (mm).

3.3 | Methods to calculate negative moment capacity

3.3.1 | PCA-method

Portland Cement Association Research and Development laboratories implemented the first major studies performed to address the issues of prestress girders with cast-in-place deck made continuous at the beginning of

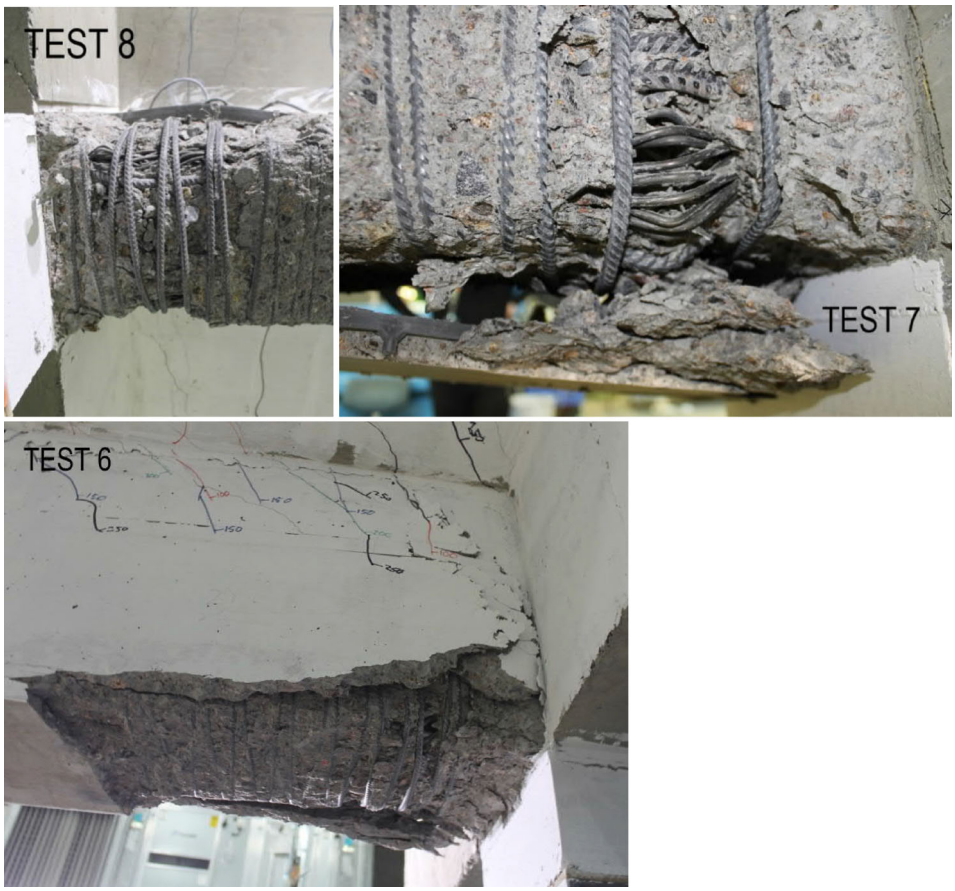

FIGURE 8 Point of fracture after test

TABLE 4 Relevant test results from test beams

Test number	x_{frac1}/x_{frac2} (mm)	M_{test} (kNm)	$M_{spalling}$ (kNm)	$M_y(x_{SGB10})$ (kNm)	Δ (mm)
5	453/328	1820	1627	1316	121
6	468/343	1822	1519	1377	110
7	419/294	1870	1393	1280	99
8	449/324	1911	1286	1454	160

1960. During the first part of the extensive research program, they presented the methods to determine the ultimate negative flexural strength of a composite continuity connection between precast girders, including prestress effects. The presented methods to determine the ultimate negative moment resistance of the cross-sections were based on the following basic assumptions

1. Plane sections remain plain.
2. Strain change in bonded reinforcement and bonded prestressing tendons, whether in tension or in compression, is the same as that in the surrounding concrete.
3. The initial strain in prestressing tendons is taken into account when assessing the stresses in the tendons (long term losses are neglected).
4. Elastic strains of cross section concrete due to a prestressing force are taken into account.[2]

The stress and strain distribution of composite cross sections is presented in Figure 9. Stress f_p in each layer of prestressed reinforcement at the ultimate moment can be calculated by the linearity of strains.

$$f_p = f_{p0} - (\varepsilon_{cu2} - \varepsilon_{ce}) E_p \frac{y_p}{x} \quad (1)$$

where y_p strand distance from neutral axis (positive below neutral axis). ε_{ce} is the concrete strain due to initial prestress at the soffit of the cross section.

Internal equilibrium of the cross section then gives:

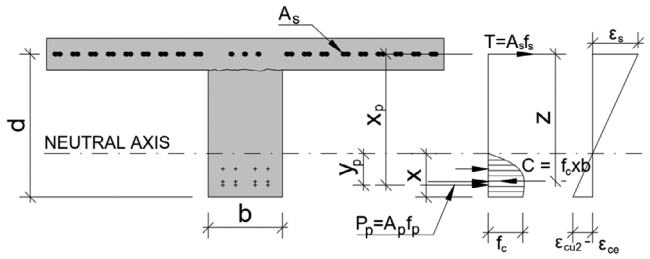

FIGURE 9 Stress and strain distribution used for flexural strength calculations

$$T = A_s f_s = C - \sum A_p f_p \tag{2}$$

where A_p is the area of prestressed steel in each layer. Ultimate moment capacity can then be calculated with Equation (3)

$$M_{Rd} = Cz - \sum A_p f_p x_p \tag{3}$$

Kaar, Kriz, and Hognestad established that, according to this analytical model, prestress force reduces the available internal compression force C, apart from a few exceptions. In other words, the more prestress force there is in the soffit of the precast beam, the less negative moment capacity it has. The concrete material model used in PCA studies was for unconfined concrete.[2] The presented method does not consider the possible change in transfer length of the bottom strands due to compression strains of the girder soffit.

The experimental results presented in previous sections Table 4 differs from the PCA methods conclusion, while the moment capacity of the test specimens increased the more the precast beams were prestressed. Because of that, in this study various material models were implemented to the PCA-method trying to estimate more accurately the function of test beams at the ULS. The next section concerns a variety of material models that were utilized in this study.

3.3.2 | Confined concrete

Hardened concrete consists mainly of aggregate particles, a bond of cement paste holds the particles together. At a certain load level, the maximum capacity of the bond is reached and microcracks occur at the interface between the aggregate particles and cement paste. If there is confinement that adds to the effect of the bond and concrete ductility, the strength can be approved.[10]

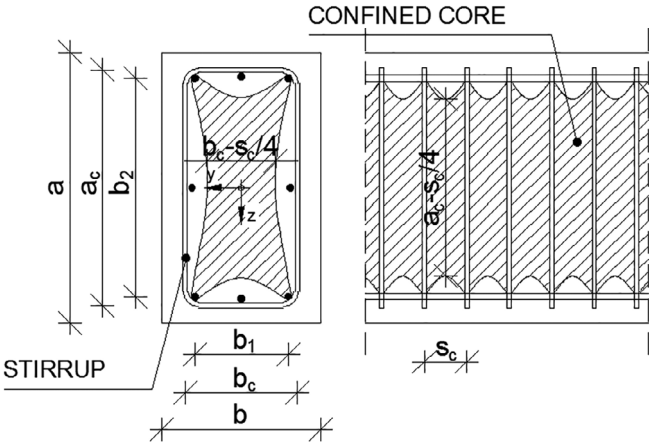

FIGURE 10 Confined and unconfined parts over the cross-section and along member with rectangular section

Concrete may be confined by transverse reinforcement. At low levels of stress in the concrete, the transverse reinforcement is hardly stressed, hence, in this case, confinement reinforcement has no effect on concrete behavior. Transverse reinforcement becomes active when concrete stresses approach its uniaxial strength. Transverse strains become high because of internal cracking and the concrete bears out against the transverse reinforcement, which applies a confining reaction to the concrete. Tests by many investigators have shown that confinement by transverse reinforcement can considerably improve the stress–strain characteristics of concrete at high strains. Test results indicate that the effect of transverse steel on concrete ductility is noticeable, it also has an effect on the strength, but such an effect is minor.[11–14]

The confining pressure σ_2 from rectangular shaped transverse reinforcement can be calculated for a tested cross-section, according to Equation (4), which is used to determine σ_2 for every confinement model discussed in this article.[15–17]

$$\sigma_2 = \rho_c f_y \alpha \tag{4}$$

$$\alpha = \left(1 - \frac{s_c}{2a_c}\right)\left(1 - \frac{s_c}{2b_c}\right)\left(1 - \frac{\sum b_i^2/6}{a_c b_c}\right) \tag{5}$$

$$\rho_c = \min\left\{\omega_y = \frac{A_{sy}}{a_c s_c}, \omega_z = \frac{A_{sz}}{b_c s_c}\right\} \tag{6}$$

where A_{sy}, A_{sz} is a cross-sectional area of confinement reinforcement parallel to the direction y,z. f_y, yield strength of confinement reinforcement. a_c, b_c, b_i, s_c (See Figure 10)

TABLE 5 Transverse reinforcements confining pressure σ_2 in test samples

Test number	Stirrup shape	ρ_c (‰)	Rebar class	s_c (mm)	a_c (mm)	b_c (mm)	$1-\frac{\sum b_i^2/6}{a_c b_c}$	σ_2 (MPa)
5	Closed-loop	6.41	B500B	75	234	418	0.44	1.09
6, 7, 8	Spiral	9.25	B500B	52	234	418	0.43	1.66

For the tested cross-sections, two different lateral supports were offered. For the prestressed concrete cross-sections, the stirrup ratio was higher than for the non-prestressed test samples. The confining pressure σ_2 for test beams is presented in Table 5.

Concrete cover outside the transverse steel is unconfined and it has stress–strain characteristics separate from core concrete. The cover concrete generally spalls when the unconfined strength is reached. This is partly also caused by the fact that heavy transverse reinforcement creates a plane of weakness that tends to precipitate spalling of the cover. Before the outermost fibers of the cross section reach the unconfined crushing strain the moment resistance of the full unspalled section is calculated neglecting any effects of confinement. After the spalling of unconfined concrete cover, the full section is replaced in the calculations by the dimensions of confined core (see Figure 10) and confined material properties are used.[12,15]

3.3.3 | Concrete stress–strain relation alternatives

Analytical calculations of ultimate flexural strength for the composite section subjected to a negative bending moment was made with several concrete material models and the results were compared with test results. The calculations were made with and without consideration of the effects of the confinement.

The unconfined material model used in the study was the parabola-rectangle stress–strain relation, according EN 1992-1-1 part 3.1.7. The model in question was chosen because confined material models found from literature can be compared best to this model in particular.

Over the past decades, several investigators have proposed stress–strain relationships for confined concrete. A few of them (eminent from a European point of view) are discussed in this article. Confinement is generally considered at the evaluation of the seismic performance of structures and it is also presented extensively in EN 1998. This article focuses on building structures, so the confined stress–strain relation of concrete introduced in references[17,18] is presented here.

$$f_{cc\_EN1998.3} = f_c\left(1+3.7\left(\frac{\sigma_2}{f_c}\right)^{0.86}\right) \tag{7}$$

$$\varepsilon_{cc\_EN1998.3} = \varepsilon_{c2}\left(1+5\left(\frac{f_{cc\_EN1998.3}}{f_c}-1\right)\right) \tag{8}$$

$$\varepsilon_{cu\_EN1998.3} = 0.004+0.5\frac{\sigma_2}{f_{cc\_EN1998.3}} \tag{9}$$

where ε_{c2} is a compressive strain in the unconfined concrete at peak stress according EN 1992-1-1 part 3.1.7.

The confinement model presented in Model Code 2010 of CEB/FIB offers increased strength and the corresponding strains according to Equations (10)–(12).[16]

$$f_{cc\_MC2010} = f_c\left(1+3.5\left(\frac{\sigma_2}{f_c}\right)^{\frac{3}{4}}\right) \tag{10}$$

$$\varepsilon_{cc\_MC2010} = \varepsilon_{c2}\left(1+5\left(\frac{f_{cc\_MC2010}}{f_c}-1\right)\right) \tag{11}$$

$$\varepsilon_{cu\_MC2010} = \varepsilon_{cu2}+0.2\frac{\sigma_2}{f_{cc\_MC2010}} \tag{12}$$

where ε_{c2} is a compressive strain in the unconfined concrete at peak stress, according to EN 1992-1-1 part 3.1.7. ε_{cu2} is the ultimate compressive strain in the unconfined concrete EN 1992-1-1 part 3.1.7.

The current EN 1992-1-1 handles confinement shortly in part 3.1.9. It provides formulas for material models, although it does not offer instructions on how to define effective lateral compressive stress σ_2 from transverse reinforcement. The confined concrete stress–strain model presented in EN 1992-1-1 is similar in style to the one presented in Model Code 1990 of CEB/FIB.[6,19]

$$f_{cc\_EN1992} = \begin{cases} f_c\left(1+5\left(\frac{\sigma_2}{f_c}\right)\right) \text{ for } \sigma_2 \le 0.05 f_c \\ f_c\left(1.125+2.5\left(\frac{\sigma_2}{f_c}\right)\right) \text{ for } \sigma_2 > 0.05 f_c \end{cases} \tag{13}$$

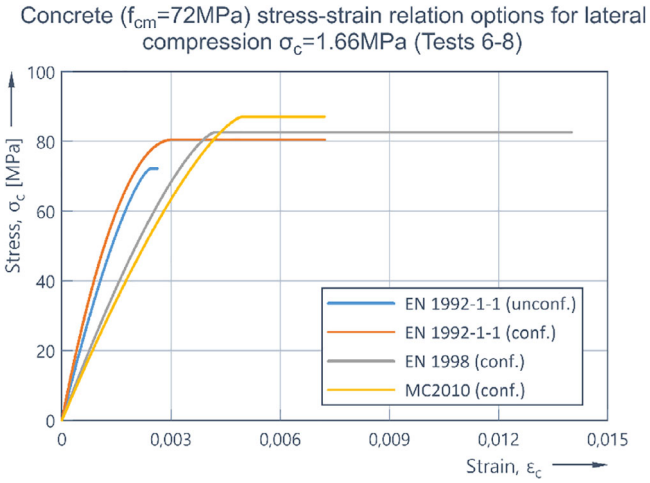

FIGURE 11 σ-ε behavior of unconfined and confined concrete, according to different material models used in this article

$$\varepsilon_{cc\_EN1992} = \varepsilon_{c2}\left(\frac{f_{cc\_EN1992}}{f_c}\right)^2 \quad (14)$$

$$\varepsilon_{cu} = \varepsilon_{cu2} + 0.2\frac{\sigma_2}{f_c} \quad (15)$$

where ε_{c2} is a compressive strain in the unconfined concrete at peak stress, according to EN 1992-1-1 part 3.1.7. ε_{cu2} is the ultimate compressive strain in the unconfined concrete EN 1992-1-1 part 3.1.7.

The second generation of Eurocodes is currently under development and draft versions and background documents of it have already being published. According to the latest draft, confinement will be dealt with more accurately and the material models will be changed towards the MC2010 model. Most recent test results indicate that the current model in EN 1992-1-1 seriously underestimates confinement.[20]

Material models of MC2010 and EN 1992-1-1 are related to the ultimate state and intended to define the maximum resistance of structure. This is in contrast to the EN 1998–3 material model which corresponds to the fullest exploitation of the deformation capacity of the structure. Figure 11 compares the four stress–strain models of the tested concrete. The lateral compressive strain used for the material models presented in Figure 11 is in accordance with the Tests 6–8.

3.3.4 | Stress–strain relations for steels

Tested cross-sections contained two types of reinforcements, according to Table 3. As flexural strength analyses made in this article, an idealized stress–strain diagram, with an inclined top branch, was used for both

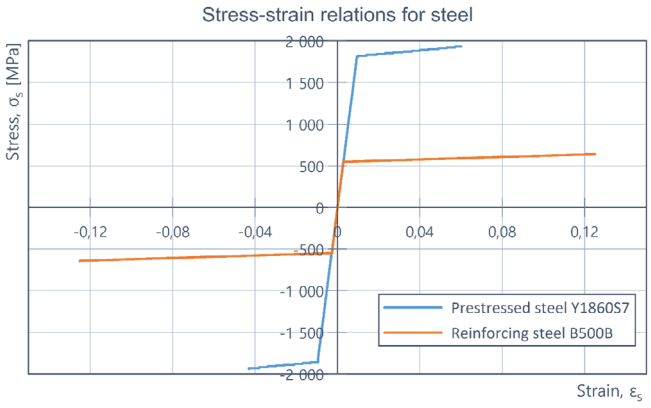

FIGURE 12 Idealized σ-ε relation of steel bars B500B and prestressed strands Y1860S7, based on measurements

prestressed and normal reinforcement steel. The stress–strain curve for steel B500B was assumed to be identical in tension and compression. Several sources have suggested that it is a reasonable assumption.[6,12] The stress–strain relation at compression for prestressing steel was defined according to Ref. 16. The stress–strain curves used in this study are presented in Figure 12.

3.3.5 | Calculated negative moment capacities

When the confined concrete properties are exploited in terms of calculations, the spalling of the cover of concrete has to be taken into account. In the calculations made in this study, the confined cores dimensions of concrete are presented in Table 6. Concrete cover spalled from each test beam, so the confined core could be measured. The width used in the calculations was the total width minus the spalled of cover and stirrup diameter.

Table 7 shows the following results for the analytical calculations made with different concrete material models presented in Section 3.3.3 of the test beams:

1. Negative flexural moment capacity M_{calc}.
2. Deck steel strain at failure ε_s.
3. Bottom row strand strain at failure ε_p.

3.4 | Comparison of tested and calculated negative moment capacities

A bar chart in Figure 13 presents the calculated ultimate moments of specimens and the comparison with experimental values. Black lines are also added to bars of experimental results to indicate the moment visible compression cracking of the beam soffit could be observed.

TABLE 6 Spalled concrete cover measurements taken from the test beams

Test number	Spalling of the cover of concrete (mm)		Width of confined core (mm)
	Side	Bottom	
5	19	25	234
6–8	19	18	234

TABLE 7 Relevant analytical calculation results from test beams

Test number	Deck slabs ρ_1 (%)	Prestressed steel in precast girders	Girder concrete strength f_{cm} (MPa)	M_{calc} (kNm) Deck steel strain ε_s (‰) Bottom row strand strain ε_p (‰) Concrete strain at cross section soffit ε_c (‰)			
				Used concrete material model			
				EN 1992-1-1 (unconf)	EN 1992-1-1 (conf)	EN 1998–3	MC 2010
5	5.1	0	72.1	$M_{calc} = 1671$	$M_{calc} = 1814$	$M_{calc} = 1833$	$M_{calc} = 1808$
				$\varepsilon_s = 2.4$	$\varepsilon_s = 4.7$	$\varepsilon_s = 10.1$	$\varepsilon_s = 4.0$
				$\varepsilon_c = -2.6$	$\varepsilon_c = -5.6$	$\varepsilon_c = -10.8$	$\varepsilon_c = -5.6$
6	5.1	4 + 2	72.2	$M_{calc} = 1532$	$M_{calc} = 1916$	$M_{calc} = 2010$	$M_{calc} = 1921$
				$\varepsilon_s = 2.1$	$\varepsilon_s = 6.1$	$\varepsilon_s = 16.0$	$\varepsilon_s = 5.5$
				$\varepsilon_p = 5.0$	$\varepsilon_p = 0.7$	$\varepsilon_p = -5.2$	$\varepsilon_p = 0.7$
				$\varepsilon_c = -2.6$	$\varepsilon_c = -7.2$	$\varepsilon_c = -14.0$	$\varepsilon_c = -7.2$
7	5.1	8 + 2	72.2	$M_{calc} = 1348$	$M_{calc} = 1880$	$M_{calc} = 2054$	$M_{calc} = 1895$
				$\varepsilon_s = 1.9$	$\varepsilon_s = 5.8$	$\varepsilon_s = 17.8$	$\varepsilon_s = 5.0$
				$\varepsilon_p = 5.3$	$\varepsilon_p = 1.0$	$\varepsilon_p = -4.9$	$\varepsilon_p = 0.6$
				$\varepsilon_c = -2.6$	$\varepsilon_c = -7.2$	$\varepsilon_c = -14.0$	$\varepsilon_c = -7.2$
8	5.1	12 + 2	72.2	$M_{calc} = 1198$	$M_{calc} = 1857$	$M_{calc} = 2060$	$M_{calc} = 1870$
				$\varepsilon_s = 1.7$	$\varepsilon_s = 5.5$	$\varepsilon_s = 18.9$	$\varepsilon_s = 4.8$
				$\varepsilon_p = 5.5$	$\varepsilon_p = 1.1$	$\varepsilon_p = -4.6$	$\varepsilon_p = 1.1$
				$\varepsilon_c = -2.6$	$\varepsilon_c = -7.2$	$\varepsilon_c = -14.0$	$\varepsilon_c = -7.2$

The bar chart shows considerable differences between calculated unconfined capacities and experimental results. According to the eurocodes unconfined material model, negative moment capacity tends to decrease, while prestress in the precast concrete beams increases, whereas experimental results show no such dependency. In contrast, experimental results indicate that an addition of prestress causes a slight increase in the ultimate capacity. Calculated values, according to confined material models, show a better correlation between analytical and tested ultimate capacities. From the chart, it can also be seen that the moment, at the time that visible cracking in precast beams compressed soffit could be observed, is comparable to analytical capacities defined by an unconfined material model.

SGB (SGB4–SGB6, SGB10–SGB12) and vertical deflection (DG1–DG5) measurement results provide detailed data regarding a beam's behavior and strain distribution at a critical section during loading. The moment curvature relation of a test beam can be analyzed with the help of this measured data. The next sections compare the measured and calculated moment curvature relations of test beams.

3.5 | Curvature distribution along a beam at ULS

With verification of the plain section assumption, the curvature φ of a small element of length can be defined according to the concrete strain in the extreme fiber $\mathcal{E}_c$, tension steel strain $\mathcal{E}_s$ and effective height d. The curvature is then

$$\varphi = \frac{\varepsilon_c + \varepsilon_s}{d} \tag{16}$$

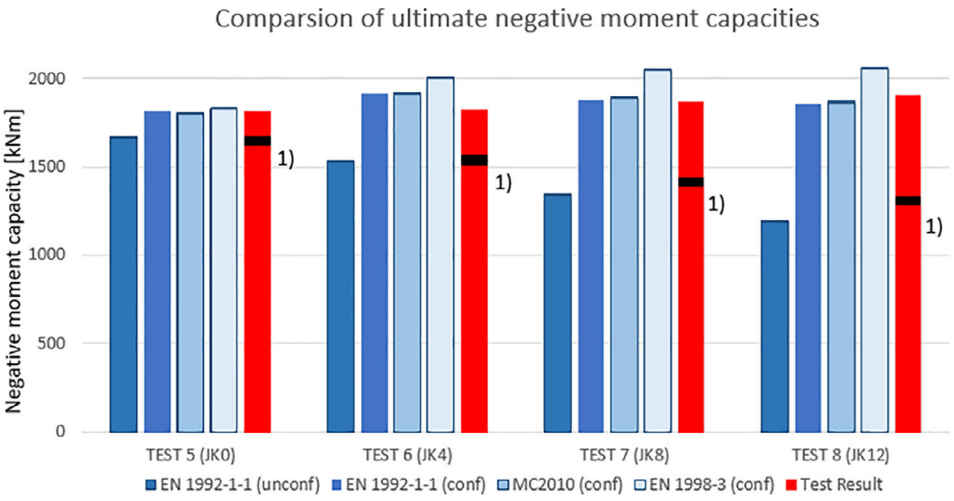

FIGURE 13 Comparison of calculated and tested ultimate negative moment capacities. 1) black line indicates the moment that a visible spalling cracking of the beam soffit could be observed

The curvature varies along the length of the member. Figure 14 shows the test member's theoretical ultimate rotation, deflection, curvature and bending moment distribution at failure. For moment values less than the yield moment M_y, the curvature increases linearly from the free end of the cantilever to the support. Inelastic curvature region is the area where either yielding of the reinforcement, or crushing of concrete, or both takes place, the plastic hinge length is the zone where the plastic curvature is assumed to be constant. This means that the real distribution of plastic curvatures, which is nearly triangular, is replaced by an idealized uniform plastic curvature over a shorter "plastic hinge length L_{pl}". The curvature fluctuates along the member because of increased stiffness of the member between the cracks. The curvature distribution at the ultimate limit state can be idealized into elastic and plastic regions (see Figure 14(d)).[21]

The Rotation θ between the cantilever beams end and support can be defined from curvature distribution along the member length. This is given by:

$$\theta = \int_0^L \varphi \, dx \tag{17}$$

Vertical deflection Δ of the cantilever beams tip is then:

$$\Delta = \int_0^L \varphi x \, dx \tag{18}$$

3.5.1 | Curvature diagram according to measured strain data

Curvatures of the test beams can be defined at measuring points SGB4 + SGB10, SGB5 + SGB11 and SGB6 + SGB12, where the strains are measured from the top and bottom part of the cross section. At the testing stage, the SGBs failed, probably due to large strains, at the load level of 75%–88% of failure load. Because of this, the curvature diagrams can be drawn only to that load level. At tests 5 and 6, one of the measuring points SGB6 or SGB12 was damaged during casting and, as a result, curvatures could not be calculated at that point at all. Curvature diagrams at different load levels, according to measured strain data, are presented in Figure 15(a-d).

From the tested curvature diagrams, it can be seen that at higher load levels the plastic area of the beam tends to increase. The maximum curvatures measured are about 0.03–0.05 1/m. It also seems that the more prestress force there is in the test beam, the earlier plastic hinge starts deform and it is longer. The length of the plastic area is less than 1.2 m in all tests.

3.5.2 | Length of plastic hinge

The length of the plastic hinge is challenging to define due to high strain localization, interaction and relative movement between constituent materials and nonlinearity of materials. Numerous techniques and models are available in literature to estimate the plastic hinge length of RC members.[17,22–26] From these models, it can be seen that the shear span, section depth, yield strength of concrete and steel and the diameter of reinforcement are the major variables.[27]

Various empirical equations and calculated plastic hinge lengths of the test beams are given in Table 8. Together, these references indicate that the length of the plastic hinge of test beams, according to expressions found from literature, varies between 319 and 823 mm.

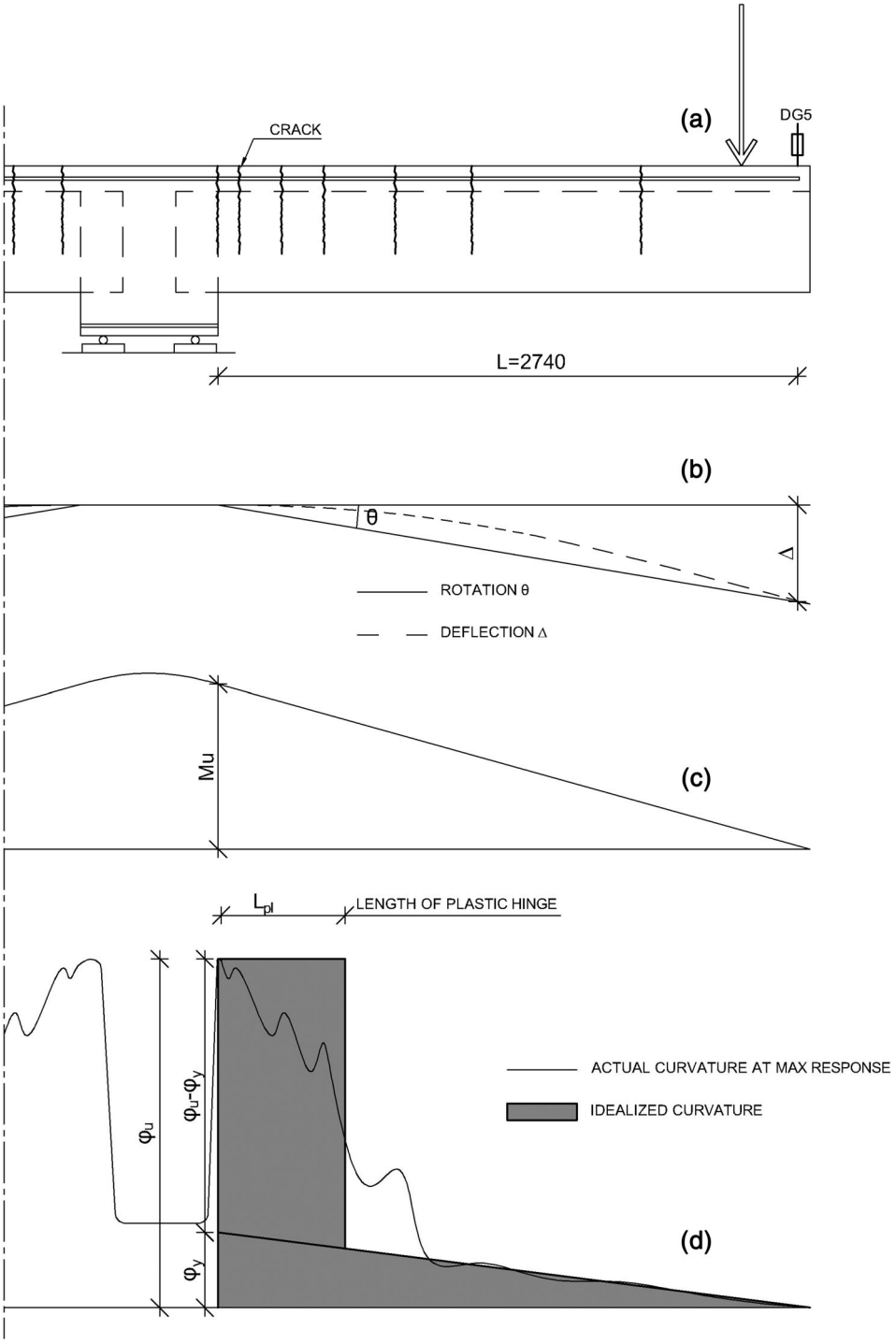

FIGURE 14 Curvature distribution along the beam at the ultimate moment (a) beam; (b) Rotation and deflection; (c) Moment; (d) Curvature diagram

According to Figure 15(a-d) and Table 8 data, there is evidence to estimate an equivalent plastic hinge length of 400–800 mm in this study.

3.5.3 | Curvature at failure calculated from vertical deflection

The deflection of a member can be calculated by integrating the curvature along the member, as presented in formula (18). Such an approach does not accurately take into consideration the effect of the tension stiffening, as well as the additional deformations caused by shear and by bond slip of the reinforcement. It is still frequently possible to obtain a reasonable agreement between computed and experimental displacements directly from the bending moment distribution and the moment-curvature relation.[12]

Curvature of the test beams cannot be defined at a final stage with the help of SGB measurements. Because

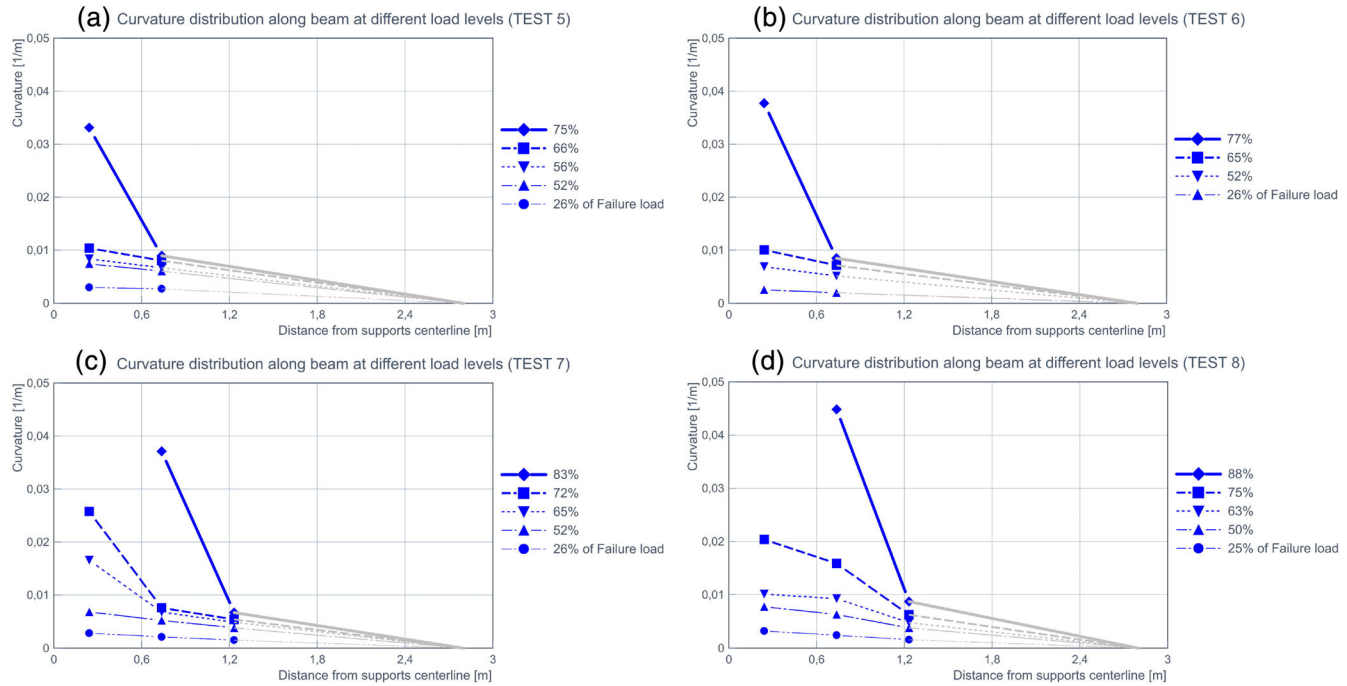

FIGURE 15 (a-d) Test specimens curvature distribution along a beam during testing at different load levels

of that, the curvature at failure is calculated based on vertical deflection measurements.

Deflection at the tip of cantilever beam can be calculated with the help of Equation (18) and idealized curvature distribution. The integral can be solved, for example, with the help of Mohr's virtual work product integration table. The vertical deflection at the tip of the cantilever beam is then:

$$\Delta = \frac{\varphi_y l^2}{3} + (\varphi_u - \varphi_y) l_{pl} \left(l - \frac{l_{pl}}{2} \right) \tag{19}$$

Then the maximum curvature φ_u can be written as:

$$\varphi_u = \frac{\Delta - \frac{\varphi_y l^2}{3}}{l_{pl}\left(l - \frac{l_{pl}}{2} \right)} + \varphi_y \tag{20}$$

When we can estimate the length of the plastic hinge and we know the maximum vertical deflection at the tip of cantilever beam and elastic stiffness of the cross-section, the maximum curvature reached at the load testing can be calculated. Inclined flexural-shear cracking increase the area in which the reinforcement is yielding (the plastic hinge zone). Thus this formulation deals indirectly also effects of shear through L_{pl}, which is not a physical but a conventional quantity.[15,26]

The calculated maximum curvature values for assumption that the length of plastic hinge is 600 mm are presented in Table 9. The elastic stiffness of the test beam is defined according to SGB measurements SGB10–SGB12 and SGB4–SGB6 made during testings elastic phase. The elastic stiffness and elastic part of the curvature of the test beams are also presented in Table 9.

3.6 | Moment-curvature relationship

One of the salient features of the flexural behavior is the moment-curvature relationship. It accurately determines the load-deformation behavior of a concrete section. Tested and calculated moment-curvature curves of test beams are illustrated and discussed in the next sections, Sections 3.6.1 and 3.6.2.

3.6.1 | M-C according test results

The strains at the critical three sections of each test beam were measured with SGBs, as the bending moment was increased to failure, the curvature could then be calculated from Equation (16).[12] At a load level of 75%–88% of failure load, SGBs failed in all tests. After that the moment- curvature relation had to be estimated with the help of displacement measurements at failure, plastic hinge length approximation and Equation (20). Figure 16(a-d) presents experimental moment-curvature relations of the tests 5 to 8. It is apparent from these curves that all of the tested beams

TABLE 8 Expressions for the plastic hinge length and L_{pl} of test girders

References	Grounds behind expression	Plastic hinge length expression (L_{pl})	L_{pl} (mm)
Paulay and Priestley[26]	• Tensile strain penetration • Inclined flexural-shear cracking	$0.08L_v + 0.022d_{bL}f_y$	400
Biskinis and Fardis[22]	• Flexure-controlled ultimate chord rotation • Monotonic loading	$h\left(1.1 + 0.04\min\left(9; \frac{L_v}{h}\right)\right)$	772
Grammatikou, Biskinis, Fardis[23]	• Flexure-controlled ultimate chord rotation • Monotonic loading	$0.34h\left(1 + 1.1\min\left(9; \frac{L_v}{h}\right)\right)\left(1 - 0.5\sqrt{\min\left(2.5; \max\left(0.05; \frac{b_w}{h}\right)\right)}\right)\left(1 - 0.5\min\left(0.7; \frac{N}{A_c f_c}\right)\right)$	747–823 depending on compression of the cross section
Jaeman Lee, Minehiro Nishuyama[24]	• Failure mode: flexural or shear after flexural yielding	h	600
EN 1998–2 (E.19)[25]	• Hinge occurring at the junction of a pier with the foundation body	$0.1L_v + 0.015f_y d_{bL}$	400
EN 1998–3 (A.5)[17]	• Compatible with EN 1992-1-1 confinement model 3.1.9 • Cyclic loading • No lapping of longitudinal bars	$0.1L_v + 0.17h + 0.24\frac{d_{bL} f_y(\mathrm{MPa})}{\sqrt{f_c(\mathrm{MPa})}}$	611
EN 1998–3 (A.9)[17]	• Compatible with EN 1998–3 confinement model (A.6)-(A.8) • Cyclic loading • No lapping of longitudinal bars	$\frac{L_v}{30} + 0.2h + 0.11\frac{d_{bL} f_y(\mathrm{MPa})}{\sqrt{f_c(\mathrm{MPa})}}$	319

Note: L_v is the ratio moment/shear at the end section, h is the depth of cross-section, $f_y f_c$ are the concrete compressive strength and reinforcement yield strength directly obtained as mean values from in-situ tests, d_{bL} bar diameter of longitudinal reinforcement, N positive for compression.

TABLE 9 Elastic stiffness EI, elastic part of curvature φ_y, and ultimate curvature φ_u of test beams defined by experimental data

Test nr	EI (MNm^2)	φ_y (1/m)	φ_u (1/m) (L_{pl} = 600 mm)
5	134	0.014	0.072
6	197	0.010	0.067
7	153	0.013	0.058
8	161	0.013	0.100

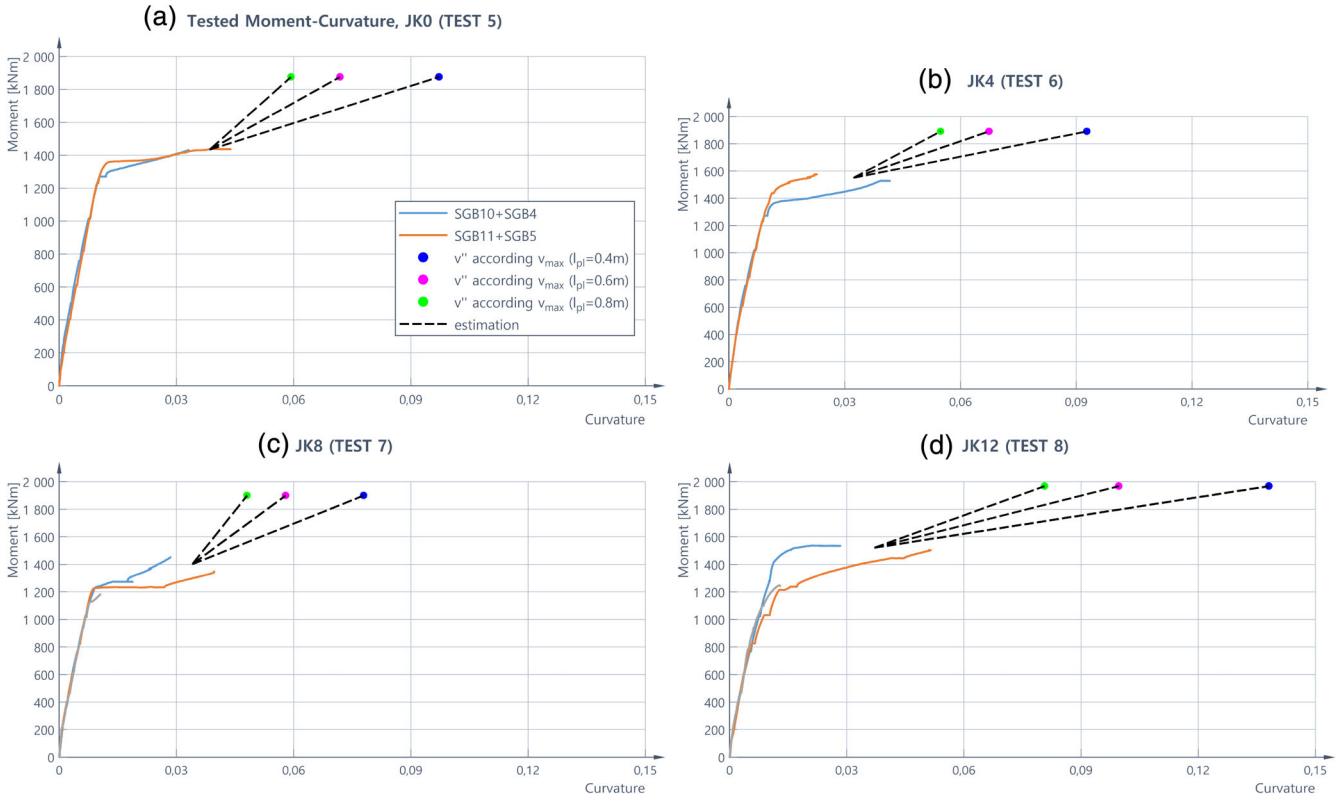

FIGURE 16 (a-d) Moment-curvature of the tested beams, according to experimental data

had a clear yielding phase and none of the beams had a brittle failure.

3.6.2 | M-C according different material models

Theoretical moment-curvatures for tested cross-sections have been derived based on calculation methods presented in Section 3.3.1 and four different concrete stress–strain relationships.

1. EN 1992-1-1 unconfined concrete.
2. EN 1992-1-1 confined concrete.
3. MC2010 confined concrete.
4. EN 1998–3 confined concrete.

Minute sensitive analysis was made regarding the impact of the compression behavior of steel and, after that, suitable stress–strain relations of steel were selected and kept the same during computations presented in this article. Exact material assumptions are determined in Section 3.3.3 and Section 3.3.4. Theoretical moment-curvature relations are presented in Figure 17(a-d).

In reality when the outermost fibers reach the crushing strain of unconfined concrete and the concrete cover spalls, the moment resistance of the section drops. This does not come out from the calculated confined moment-curvature relations shown in Figure 17(a-d). This is due that the confined material model calculations presented here are made only for confined core.[15]

Tested cross-sections are heavily reinforced. What stands out in the theoretical moment-curvature

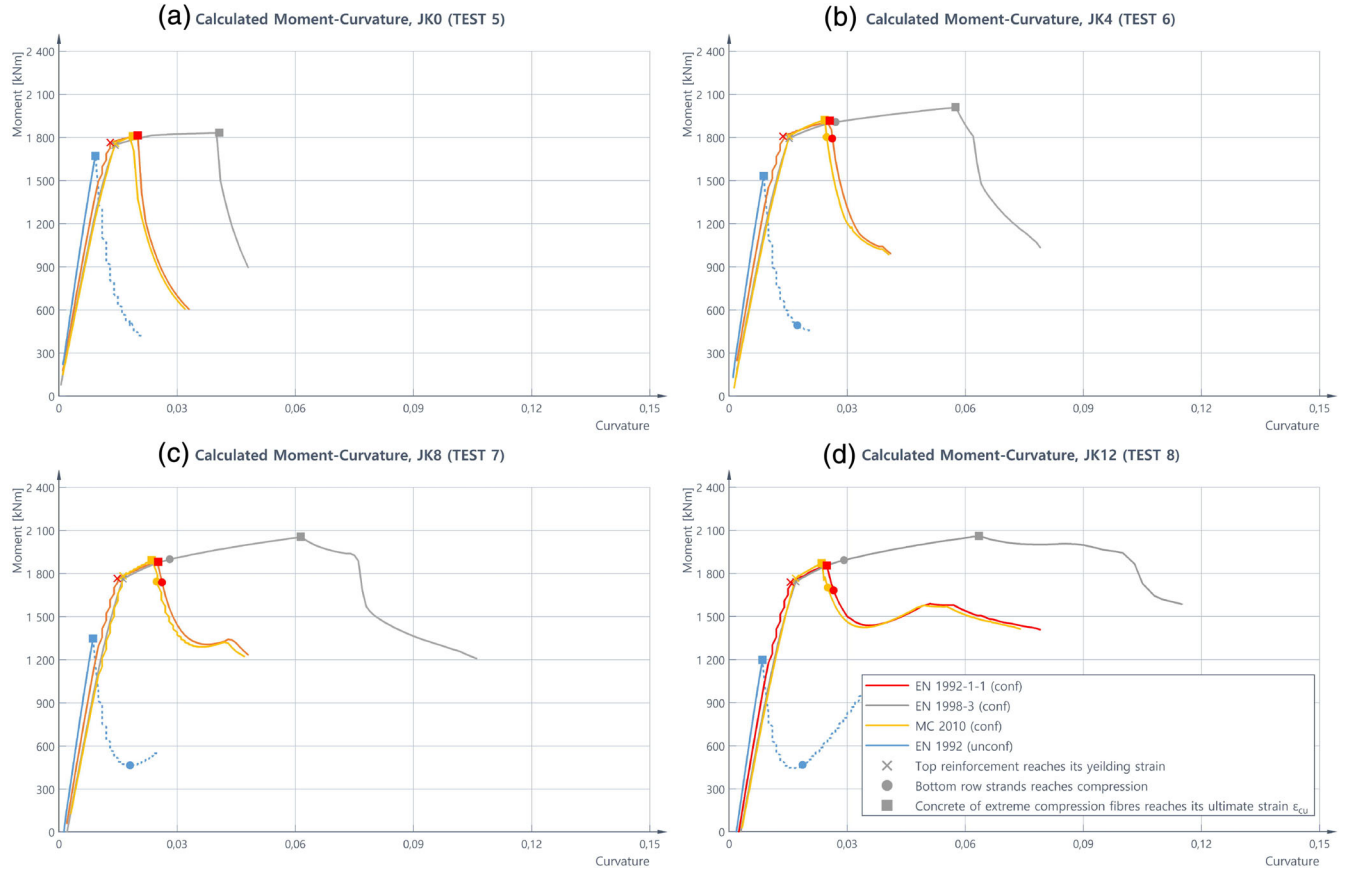

FIGURE 17 (a-d) Analytical moment-curvatures of the tested beams, according to different material models

relationships is that, if the used material model is unconfined, the concrete crushes at a relatively insignificant curvature prior to the steel yields, causing a sharp decrease in the moment capacity. This differs from that of all the confined curves which illustrate obvious ductile behavior, regardless of the fact that the cross sections are over-reinforced.[12]

For unconfined material model maximum theoretical curvature remains under 0.01 in all tests, while in confined models the ultimate curvature varies between 0.03 and 0.11. The difference between the curves is considerable.

It can be seen from the Figure 17(a-d), that in confined theoretical analyses cross sections bottom strands act in the final stage as compressive reinforcement and this increases its ductility significantly. At this point concrete cover has spalled of and bond of bottom strands is damaged. It is not also certain how pretension strands act under compression. Although calculated moment-curvature relations are similar to experimental results shown in Figure 16(a-d), end parts of calculated these relations therefore need to be interpreted with caution. The curves based on *Eurocode 8: Design of structures for earthquake resistance* confined material model is the most ductile.

4 | CONCLUSONS

The aim of the present research was to examine experimentally the negative moment capacity of precast prestressed beams continuity connections and compare test results to the analytical models. This article set out to evaluate what influence such a high reinforcement ratio and precast beams prestress force has on connections mode and ductility of flexural failure. The conclusions of this study can be presented as follows:

1. The degree of prestressing force of the connected prestressed girders did not have a significant effect on the ultimate load of tested continuity connections.
2. The amount of prestress force did, however, effect the structure's behavior on high-load levels. The concrete cover of the strongly compressed soffit of the beam began to spall at considerably lower load levels compared to the failure load. The higher the prestressing ratio that the connected precast beams had, the less load was needed to cause visible cracking at the bottom part of critical sections. The moment, at the time that visible cracking in precast beams compressed soffit could be observed, was

comparable to calculated capacities defined by unconfined material model.

3. General yielding of the deck reinforcement steel developed over the support of all test girders well prior to ultimate strength was reached regardless of prestress effects and the fact that the connection was over-reinforced. The tested moment-curvature relationships indicate that the failure of the connection was ductile. The distribution of moments would have taken place in statically indeterminate girders with the joint in question.
4. A critical section that reached ultimate strength first was approximately the same location in which prestress force reached its transfer length and became fully effective. Failure always took place outside the diaphragm.
5. From the spalling, crushing, and deformations of the structure, it can be concluded that confinement had a remarkable role on the behavior of tested connections near failure. Tightly spaced stirrups created confinement to the cross-section core after the concrete cover had spalled off. At this stage cross section had considerably capacity left. Calculated and tested moment-curvature relations and moment capacities of the connection have been compared. The results show that material models operate as they are intended to. It has been found that confined concrete material models, according to Model Code 2010 and EN 1992-1-1, are the most accurate to analyze the failure load of continuity connections while the confined model, according to EN 1998–3, is the best to predict the deformability of the structure near failure.
6. The results of this investigation indicate that in the design of continuity connection, unconfined concrete material model should be considered, and the effect of prestress force cannot be neglected in negative moment capacity calculations. After reaching ultimate capacity, according to these assumptions, the structure has still considerable robustness left.
7. The half-scale sample size might have increased the importance of confinement to the connection's failure mode. More experimental research using larger cross-sections would be useful to establish a greater degree of accuracy on this matter.

ACKNOWLEDGMENTS

The authors gratefully acknowledge the financial support provided by the Finnish Concrete Industry. The authors would also like to thank Mr. Jani Kujala for his assistance in the laboratory phase of this study.

DATA AVAILABILITY STATEMENT

Data available on request from the authors.

ORCID

Ulla Kytölä https://orcid.org/0000-0003-0645-8146
Olli Asp https://orcid.org/0000-0003-4022-8336

REFERENCES

1. Jayanandana, C. A. D. (1989). Continuity development between precast beams using prestressed slabs, and its effect on flexure and shear. The University of Leeds.
2. Kaar PH, Kriz LB, Hognestad E. Precast-prestressed concrete bridges 1. Pilot tests of continuous girders. J PCA Res Devel Lab. 1960;2:21–37.
3. Mattock BAH, Kaar PH. Precast-prestressed concrete bridges 3. Further tests of continuous girders. J PCA Res Devel Lab. 1960;2:51–78.
4. Oesterle, R. G., Glikin, J. D., & Larson, S. C. (1989). Design of precast prestressed bridge girders made continuous. Washington D.C.
5. Miller, R., Castrodale, R., Mirmiran, A., & Hastak, M. (2004). NCHRP report 519, connection of simple-span precast concrete girders for Continuity. Washington.
6. SFS-EN 1992-1-1. (2005). Eurocode 2: Design of concrete structures. Part 1–1: General rules and rules for buildings.
7. Newhouse, C. D. (2005). Design and behaviour of precast, prestressed girders made continuous - an analytical and experimantal study. Virgiana Polytechnic Institute and State University.
8. FIB. (2012). Fib Bulletin 65: Model Code 2010, Final draft - Volume 1. International Federation for Structural Concrete (fib).
9. Russell, B., Burns, N., & Kreger, M. (1991). Measurement of transfer length in prestressing strands in prestressed concrete specimens.
10. FIB. (2009). Fib Bulletin 51, Structural Concrete, Textbook on behaviour, design and performance, Second Edition, Volume 1. International Federation for Structural Concrete (fib).
11. Mander JB, Priestley MJN, Park R. Theoretical stress-strain model for confined concrete. J Struct Eng. 1989;114:1804–26.
12. Park R, Paulay T. Reinforced concrete structures. New York, NY: John Wiley & Sons; 1975.
13. Roy, H. E. H., & Sozen, M. A. (1964). Ductility of concrete. Paper presented at: International Symposium on the Flexural Mechanics of Reinforced Concrete, ASCE - ACI. Miami.
14. Scott BD. Stress-strain relationships for confined concrete: rectangular sections. New Zeland: Christchurch; 1980.
15. Fardis, M. N. (2009). Seismic design, assessment and retrofitting of concrete buildings: based on EN-Eurocode 8. https://doi.org/10.1007/978-1-4020-9842-0
16. FIB. (2012). Fib Bulletin 66, Model Code 2010, Final draft, Volume 2. Lausanne, Switzerland: International Federation for Structural Concrete (fib).
17. SFS-EN 1998–3. (2005). Eurocode 8: design of structures for earhtquake resistance. Part 3: assessment and retrofitting of buildings. CEN, European Committee for Standardization.
18. SFS-EN 1998–1. (2005). Eurocode 8: Design of structures for earhtquake resistance. Part 1: General rules, seismic actions and rules for buildings.
19. CEB-FIB. (1993). Model code 1990, Design code. London, England.
20. ISO. (2010). SRC GR14. 1–67. NWIP 16527. https://doi.org/ISO/TC215/N796.

21. Borg, R. C. (2015). The deformation capacity of reinforced concrete elements subject to seismic loading: determination of empirical equations for assessment. University College London.
22. Biskinis, D., & Fardis, M. N. (2009). Deformations of concrete members at yielding and ultimate under monotonic or cyclic loading (including repaired and retrofitted members).
23. Grammatikou S, Biskinis D, Fardis MN. Flexural rotation capacity models fitted to test results using different statistical approaches. Struct Concr. 2018;19:608–24. https://doi.org/10.1002/suco.201600238
24. Lee J, Nishiyama M. Strength and deformation capacity at failure of post-tensioned precast concrete members Jaeman. Struct Eng Int. 2018;25:282–91. https://doi.org/10.2749/101686615X14210663188817
25. SFS-EN 1998–2. (2006). Eurocode 8: Design of structures for earhtquake resistance. Part 2: Bridges.
26. Paulay T, Priestley MJN. Seismic design of reinforced concrete and masonry buildings. Vol 25. Hoboken, NJ: A Wiley Interscience publication; 1992. https://doi.org/10.5459/bnzsee.25.4.362
27. Zhao X, Wu YF, Leung AY, Lam HF. Plastic hinge length in reinforced concrete flexural members. Proc Eng. 2011;14:1266–74. https://doi.org/10.1016/j.proeng.2011.07.159
28. Kujala, J. (2020). Prestressed concrete girders made continuous - continuity tests. Tampere University.

AUTHOR BIOGRAPHIES

Ulla Kytölä, Ph. D. student
Unit of Concrete and Bridge Structures
Tampere University
Tampere, Finland
ulla.kytola@tuni.fi

Olli Asp, Ph. D. student
Unit of Concrete and Bridge Structures
Tampere University
Tampere, Finland
olli.asp@tuni.fi

Anssi Laaksonen, Professor
Unit of Concrete and Bridge Structures
Tampere University
Tampere, Finland
anssi.laaksonen@tuni.fi

How to cite this article: Kytölä U, Asp O, Laaksonen A. Negative bending tests on precast prestressed concrete beams made continuous. Structural Concrete. 2021;1–20. https://doi.org/10.1002/suco.202100043